

# Negative thermal expansion of water in hydrophobic nanospaces

Ryusuke Futamura, Taku Iiyama, <sup>\*</sup> Atom Hamasaki, Sumio Ozeki

*Department of Chemistry, Faculty of Science, Shinshu University, 3-1-1 Asahi, Matsumoto,  
Nagano 390-8621, Japan*

<sup>\*</sup>Corresponding author

## **Abstract**

The density and intermolecular structure of water in carbon micropores ( $w = 1.36$  nm) are investigated by small-angle X-ray scattering (SAXS) and X-ray diffraction (XRD) measurements between 20 K and 298 K. The SAXS results suggest that the density of the water in the micropores increased with increasing temperature over a wide temperature range (20–277 K). The density changed by 10%, which is comparable to the density change of 7% between bulk ice ( $I_c$ ) at 20 K and water at 277 K. The results of XRD at low temperatures (less than 200 K) show that the water forms the cubic ice ( $I_c$ ) structure, although its peak shape and radial distribution functions changed continuously to those of a liquid-like structure with increasing temperature. The SAXS and XRD results both showed that the water in the hydrophobic nanospaces had no phase transition point. The continuous structural change from ice  $I_c$  to liquid with increasing temperature suggests that water shows negative thermal expansion over a wide temperature range in hydrophobic nanospaces. The combination of XRD and SAXS measurements makes it possible to describe confined systems in nanospaces with intermolecular structure and density of adsorbed molecular assemblies.

## 1. Introduction

Water is ubiquitous, and it is the one of the most interesting chemical substances because of its unique physical properties.<sup>1-5</sup> One of its best-known anomalous properties is its density maximum at 277 K. In bulk conditions (1 bar, 298 K), each water molecule has 4.4 nearest neighbours, compared to 4 nearest neighbours in the ice  $I_h$  structure. Thus, liquid water is denser than bulk ice. The liquid water is believed to exist inside tetrahedral structures as ice, and some molecules fall into interstitial spaces in the tetrahedral structure. Instead of the volume decrease typical at decreasing temperatures, water exhibits negative thermal expansion between 273 K and 277 K and in supercooled water, which causes the density maximum at 277 K. Thus, we should consider the intermolecular structures (i.e., hydrogen bond networks) of water when we examine its unique features.

The behaviour of water in nanospaces has attracted considerable interest.<sup>3, 6-10</sup> The properties and structures of molecular assemblies in nanospaces differ greatly from those in the bulk because of the different conditions in nanospaces. The confinement effects that cause these differences arise from spatial limitations, the large potential fields due to adsorbents, and quasi high pressure effects. For example, Kaneko et al. showed that NO molecules form dimers at 298 K in carbon micropores, although it is a supercritical gas at that temperature in the bulk gas phase.<sup>11</sup> Many other observations have been reported.<sup>12-16</sup> In addition to the confinement effects, water assemblies in nanospaces are strongly influenced by the hydrophobicity of the pore walls. The adsorption isotherm of water on hydrophobic microporous materials is of type V in the IUPAC classification, although those of many gaseous molecules are of type I.<sup>17</sup> This indicates that water behaves peculiarly in hydrophobic nanospaces.

In situ X-ray scattering methods are a powerful tool for describing fluid behaviour in confined spaces because X-ray scattering supplies information on intermolecular structures. We have employed in situ X-ray diffraction (XRD) to demonstrate that water assemblies form ice-like intermolecular structures in carbon micropores even at ambient temperature.<sup>6</sup> Moreover, we applied small angle X-ray scattering (SAXS) methods to a water-activated carbon fiber adsorption system and successfully confirmed the formation of cluster-like assemblies. The size of water assembly is around 0.9 nm at the initial stage of adsorption, and then gradually increases with adsorbed amount.<sup>7</sup>

The confined water attracts much attention with relevance to polymorphism of supercooled water in low temperature, which is not accessible experimentally in the bulk.<sup>18,19</sup> It is expected that the nanoporous structure expand the accessible region of super-cooled water to low temperature region.<sup>20</sup> Liu et al.<sup>21,22</sup> reported an anomalous temperature dependence of water density in MCM-41 using small-angle neutron scattering (SANS) measurements, demonstrating that water can be supercooled to at least 160 K and has a density minimum at 210 K in MCM-41. Moreover, Zhang et al.<sup>23</sup> examined the behaviour of water in CMK-1, a mesoporous carbon synthesized using MCM-48-S mesoporous silica as a template.<sup>24, 25</sup> They demonstrated that the density minimum does not appear, and the density decreases monotonously with decreasing temperature after a maximum at 260 K. These differences are attributed to the surface hydrophilicity of the materials and are very important not only for basic science but also for applications of porous materials (e.g., electrical double-layer capacitors<sup>13, 26</sup>). However, these papers did not report detailed microscopic views, which are necessary to obtain a more precise understanding of the behaviour of water in nanospaces.

In this paper, we investigated the temperature dependence of the density and intermolecular structure of water assemblies in carbon micropores. We used in situ XRD and SAXS measurements, which allowed us to describe the behaviour of water confined in nanospaces having various pore geometries at the micro- and mesoscopic levels. We used an activated carbon fiber as an adsorbent; such fibers have well defined slit-like carbon micropores and can be provide various pore-width samples. It was frequently used for basic research on fluids in carbon nanospaces.<sup>7, 12, 27-30</sup> Unlike MCM-41 and template carbons, activated carbons do not exhibit Bragg peaks in small-angle regions because of the random conformations of the graphene sheets. The equations and method used to determine the density of the confined phase, which were derived by Liu et al., use the intensity of the Bragg peaks, and so cannot be applied to porous amorphous materials such as activated carbon. However, such density data would be very useful because of the high demand for activated carbon for use in various applications. Therefore, we proposed a new equation for determining the density of the confined phase in the micropores of activated carbon fibers based on Debye–Bueche analysis.<sup>28, 29</sup>

## 2. Experimental

Activated carbon A25 (Ad'all Co. Ltd., Uji, Japan) was used as the adsorbent. This fiber-shaped pitch based activated carbons have considerably uniform pore and low surface functional groups, compared with conventional activated carbons.<sup>8</sup> Its micropore structures were determined by obtaining an N<sub>2</sub> adsorption isotherm at 77 K using a gravimetric apparatus. A water adsorption isotherm was also measured at 298 K using a volumetric apparatus. The sample was ground and preheated at 393 K and 1 mPa for 3 h before the

adsorption isotherm and in situ XRD measurements. Milli-Q water obtained by filtration of distilled water with a Milli-Q lab water system (Millipore Japan Co.) was used as the adsorbate.

We used an in situ X-ray measurement chamber that was connected to a cryostat and adsorption line for controlling the temperature and water vapor pressure of the sample. The ground sample was packed into a 1 mm thick slit-shaped cell with beryllium windows. During the in situ XRD and SAXS measurements, water vapor was introduced into the sample chamber until the A25 reached a fractional filling of  $\phi = 0.85$  at 277 K. The fractional filling was defined as the ratio of the micropore volume filled by water molecules to the maximum micropore volume, which was determined by N<sub>2</sub> adsorption isotherm measurements at 77 K. After the sample reached equilibrium, it was cooled to 20 K at 2 K min<sup>-1</sup>. Then, the SAXS and XRD (CuK $\alpha$ , 40 kV, 30 mA) were measured by the transmission method using an angle-dispersion diffractometer (Ultima III, Rigaku Co., Tokyo, Japan). Measurements were made at several temperatures as the samples were heated at 1 K min<sup>-1</sup>. The measurement ranges of SAXS and XRD were  $s = 0.36\text{--}4.26$  and  $2.84\text{--}60.09$  nm<sup>-1</sup>, respectively. These X-ray scattering measurements were conducted for 6 h (XRD, 4 h; SAXS, 2 h) at each measurement temperature.

### 3. Results

#### Pore structure and adsorption of water and N<sub>2</sub>

Figure 1 shows the N<sub>2</sub> and water adsorption isotherms of A25 at 77 K and 298 K, respectively. Table 1 lists the specific surface area  $a_\alpha$ , micropore volume  $V_0$ , and average pore width  $w$ , which were determined from the  $\alpha_s$  plots.<sup>24</sup> The N<sub>2</sub> isotherm was of type I,

which indicates that A25 is microporous, although the pore size is relatively large for micropores ( $w = 1.36$  nm). On the other hand, the water isotherm was of type V, with a large hysteresis loop at high relative pressure. The isotherm of water shows a very sharp desorption. It suggests that the water molecular assemblies have uniform curvature at the desorption process. The apparent density of adsorbed water in A25, which was determined from the saturated adsorbed amount of water and the pore volume  $V_0(\text{N}_2)$ , was  $0.92 \text{ g mL}^{-1}$ . This suggests a low density of adsorbed water compared to that in the bulk condition at 298 K ( $0.997 \text{ g mL}^{-1}$ )

### **SAXS profiles during water adsorption**

The SAXS measurements provided structural information at the semi-micro order, such as the sizes and shapes of molecular assemblies. Iiyama et al. reported changes in the density fluctuation and correlation length with water adsorption as determined by SAXS measurements; these changes suggested the formation of cluster-like molecular assemblies of water in a hydrophobic space.<sup>7</sup> In A25 ( $w = 1.36$  nm), we found that the intensity of X-ray scattering at small angles ( $2\theta < 2^\circ$ ) increased and then decreased with water adsorption (see Fig. S1). This is the same tendency as in the previously reported cluster formation, so we conclude that water molecules form molecular assemblies in the hydrophobic micropores of A25.

The strong X-ray scattering intensity in the small-angle region of the adsorption system is caused by the large density differences between the adsorption phases and the solid phases making up the adsorbents. Thus, they provide direct information about the density of the adsorption phases. Figure 2 shows the temperature dependence of the SAXS profiles of water-adsorbed A25 at  $\phi = 0.85$ , at which water molecules almost completely filled the

micropores. The SAXS intensities decreased monotonously and continuously with increasing temperature in the entire measurement region, except at 277–298 K. This suggests that the average density of the adsorbed phase in A25 increases continuously with increasing temperature below 277 K. Interestingly, the fact that the SAXS intensity above 277 K had the opposite tendency with increasing temperature suggested that water assemblies confined in carbon micropores have a density maximum around 277 K, as in the bulk conditions. Although a detailed investigation is needed in order to determine the precise temperature at which the maximum density of confined water occurs, experiments in this high-temperature region are difficult because the saturated vapor pressure of water is very sensitive to temperature in this region. We plan to discuss the precise behaviour of confined water at high temperatures under isostere conditions in the near future.

### **Debye–Bueche analysis of SAXS data**

The SAXS profiles clearly indicated a monotonous density increase with increasing temperature, or negative thermal expansion of water, in confined hydrophobic spaces over a wide temperature range between approximately 20 and 277 K. A more detailed analysis was made in order to determine the density of the confined water. We used Debye–Bueche analysis,<sup>31, 32</sup> which is a structural analytical method used for disordered materials with a bicontinuous model. We have successfully described water cluster formation in carbon micropores using this method.<sup>7, 34</sup> Here, we provide a brief overview of Debye–Bueche analysis and use it to derive the density of the adsorbed phase.

We assume a bicontinuous system consisting of a solid phase and an adsorbed phase (or vacant pores), whose densities and volume fractions are  $\rho_s$ ,  $\rho_a$ ,  $\phi_s$ , and  $\phi_a$ , respectively. If we imagine an infinite number of measurement probes of length  $r$  placed on the system at

random, we can define the probabilities of which phases each edge of the probes are resting on as a function of  $r$ . They are expressed as  $P_{aa}$ ,  $P_{sa}$ ,  $P_{as}$ , and  $P_{ss}$ , respectively. In Debye–Bueche analysis, these probabilities are represented by an exponential term  $\exp(-r/\xi)$ , where  $\xi$  is the correlation length of the system. Thus, the SAXS intensity  $I(s)$  near  $s = 0$  is given by

$$\begin{aligned}
I(s) &= 4\pi V \phi_s \phi_a (\rho_s - \rho_a)^2 \int_0^\infty r^2 \exp\left(-\frac{r}{\xi}\right) \frac{\sin(sr)}{sr} dr \\
&= 4\pi V \phi_s \phi_a (\rho_s - \rho_a)^2 \frac{2\xi^3}{(1 + \xi^2 s^2)^2} \\
&= \frac{I_0}{(1 + \xi^2 s^2)^2} \quad \dots(1)
\end{aligned}$$

where  $V$  is a constant, and  $I_0$  is the zero-angle scattering intensity, which is directly related to density fluctuations in the system. The system's two physical quantities,  $\xi$  and  $I_0$ , can be determined from the slope and intercept of  $s^2$  vs.  $I^{-1/2}$  plots, or so-called Debye–Bueche plots. By transforming this equation, we can obtain the average density of the adsorbed phase  $\rho_a$ .

$$\rho_a = \rho_s - \sqrt{\frac{I_0}{8\pi V \phi_s \phi_a \xi^3}} \quad \dots(2)$$

Here, we derived the constant  $V$  for this equipment ( $= 212.9 \text{ c.p.s. mol}^{-2} \text{ m}^3$ ) from a SAXS measurement of A25 under vacuum, and we determined the volume fraction from the adsorption isotherm measurements ( $\phi_s = 0.260$ ,  $\phi_a = 0.636$ ). For the electron density of the solid phase, we used the value for graphite ( $\rho_s = 1.135 \text{ mol cm}^{-3}$ ).

Figure 3 shows the Debye–Bueche plots of the SAXS profiles of water-adsorbed A25 at the measurement temperatures. The plots show good linearity at  $2 < s^2 < 6$ , which indicates that the systems agree well with the Debye–Bueche assumption (Debye–Bueche plots of the entire measurement region are shown in Fig. S2). Then we obtained the  $I_0$  and  $\xi$  values at each

temperature (Figs. S3 and S4). The value of  $I_0$  changed dramatically with temperature, although  $\xi$  changed little. Moreover, we applied eq. (2) to these results in order to elucidate the density of the adsorption phase and its temperature dependence, as shown in Figure 4. As the SAXS profiles show, the density of the adsorbed water increased continuously with increasing temperature below 277 K, reached a maximum around 277 K, and then decreased. This tendency agrees well with the results for mesoporous carbon obtained by Zhang et al.,<sup>20</sup> but the change in density (10%) is approximately half of that for the mesoporous carbon. Furthermore, we confirmed the absence of the density minimum around 210 K in the carbon micropores of A25, which differs from the results for the hydrophilic nanospaces of MCM-41.<sup>18,19</sup>

These results indicate that the observed behaviours are features of water in hydrophobic nanospaces. Notably, the water confined in carbon micropores showed increasing density with increasing temperature over a wide temperature range. The density difference between 20 and 277 K is 10%, which is close to the 7% density difference between bulk ice and bulk water.<sup>34</sup> The density of confined water at ambient temperature and low temperatures became less than that of the bulk state, which might imply that the hydrogen bond networks are distorted by confinement effects. Therefore, it is meaningful to investigate the intermolecular structure with XRD measurements.

### **XRD profiles during water adsorption**

Figure 5 shows the temperature dependence of the XRD profiles of water-adsorbed A25 at  $\phi = 0.85$ . The profile of A25 under vacuum at 298 K is also shown for comparison. The sharp peaks such as those at  $s = 32$  and  $36 \text{ nm}^{-1}$  came from the beryllium windows. The XRD profile of A25 shows one shoulder and two peaks at  $16, 31, \text{ and } 36 \text{ nm}^{-1}$ , corresponding

to the (002), (10), and (11) planes of micro-graphite, respectively. The XRD profile changed dramatically as water was adsorbed at 298 K (light green line) and as the temperature changed.

We subtracted the scattering intensity of A25 itself from the water-adsorbed profile to extract the scattering from adsorbed water alone.<sup>16</sup> Figure 6 shows the XRD profiles of the adsorbed water in A25 micropores at each temperature. At 298 K, a peak and a shoulder appear at  $s = 19$  and  $30 \text{ nm}^{-1}$ , respectively, indicating the formation of intermolecular water structure in A25. Moreover, the peak located at  $19 \text{ nm}^{-1}$  became sharper and shifted to a low angle with decreasing temperature. This indicates that the intermolecular distance of water increased with decreasing temperature. The XRD profiles changed continuously with temperature even at 20 K, suggesting that water does not have a clear freezing point in A25.

It is very interesting to compare these XRD profiles with those of bulk ice crystals. The XRD peaks of bulk ice  $I_h$  and  $I_c$ <sup>35</sup> are shown in Figure 6 for comparison. The peaks of confined water are broader than those of bulk crystals even at 20 K because water could not form large crystallites owing to the limited space in the micropores. The positions of the first (and strongest) peak at  $17 \text{ nm}^{-1}$  and the peaks at  $28$  and  $32 \text{ nm}^{-1}$  for confined water at 20 K correspond to the bulk  $I_c$  peaks. Furthermore, the other  $I_c$  peaks, located at  $39, 43, 48,$  and  $51 \text{ nm}^{-1}$ , can be recognized. This reveals the small-dimensional structural ordering of water in carbon micropores. Thus, the XRD profile of confined water in carbon micropores at low temperatures indicates the formation of the  $I_c$  structure. Note that the intensity of these peaks (especially those at  $28$  and  $32 \text{ nm}^{-1}$ ) decreases gradually with decreasing temperature over a wide range, disappearing around 220 K.

Yamaguchi et al.<sup>36</sup> demonstrated that water in activated carbon having 2.04 nm mesopores forms the ice  $I_h$  structure at 243 K, in contradiction to our results. The  $I_h$  peaks observed by

Yamaguchi et al. were too sharp to form in carbon micropores, indicating that water can form the  $I_h$  structure not in micropores but in mesopores or macropores, which are present in activated carbon. Morishige et al.<sup>37</sup> investigated confined water in mesoporous silicas and reported that small crystallites of hexagonal ice that contain stacking faults due to the spatial limitation exhibited  $I_c$  peaks. We conclude that the intermolecular structure of confined water changes continuously with temperature and that very small crystallites with structural faults form at low temperatures (below 220 K) in the 1.36 nm carbon micropores of A25.

### **Radial distribution function of confined water**

The structural changes with temperature reported above can be interpreted in terms of the electron radial distribution functions (ERDFs), which can be obtained from Fourier transformation of the X-ray profiles. The temperature dependence of the ERDFs of water molecules in A25 micropores at  $\phi = 0.85$  are shown in Figure 7, which also shows the ERDFs of bulk water at 298 K. Details of the ERDF derivation were provided in our previous work.<sup>16</sup>

The ERDF of bulk water shows three peaks at 0.30, 0.42, and 0.70 nm, corresponding to the first, second, and third nearest neighbours of water molecules, respectively. This indicates that water does not possess long-range order longer than 0.8 nm. On the other hand, confined water in A25 micropores at 298 K exhibited another peak at 1.0 nm. Water confined in smaller pores exhibits a higher peak for the second nearest neighbour than for the first, even at ambient temperature.<sup>6</sup> Iiyama et al. therefore concluded that water molecules confined in carbon micropores form ice-like intermolecular structure even at ambient temperature. In our results for A25, the intensities of the first and second nearest peaks are almost the same at 298 K. The first peak gradually decreases and the second peak gradually

increases with decreasing temperature. Furthermore, the intensities of the third and fourth nearest neighbouring peaks increase with decreasing temperature. Therefore, the domain size of the hydrogen bond network increased with decreasing temperature, although it remained smaller than the pore space.

### **Structural changes in confined water with changing temperature**

The XRD and SAXS results indicate that structural changes occurred in confined water in 1.36 nm hydrophobic micropores. The confined water formed an ordered structure compared with that of the bulk state at 298 K, and its density is smaller than that of bulk water. The structure of the confined water changed gradually with decreasing temperature, forming an  $I_c$ -like structure below 220 K, although the domain size is small. The fact that the intensities of the  $I_c$  peaks in the XRD profiles change over a wide temperature region (120–220 K) indicates that the confined water in this system does not show a clear phase transition point into ice. The SAXS profiles clearly showed that the confined water increased continuously in density below 277 K. The negative thermal expansion of bulk water at 273–277 K and of supercooled water below 273 K has been explained by a model in which some water molecules remain in ice structures whereas others fall into the interstitial spaces of the tetrahedral structure of water as a liquid. The radial distribution function for confined water clearly indicates an increasing number of nearest neighbour molecules with increasing temperature in a very wide temperature range.

Omichi et al. reported nuclear magnetic resonance measurements indicating the existence of unfrozen water layers on an activated carbon surface at low temperature.<sup>25</sup> This information is very useful here. The 1.36 nm pores in our investigation correspond to 4.9 molecular layers of water. In a previous investigation of 0.75 nm (2.7 layers) and 1.13 nm

(4.0 layers) pores, confined water did not show a sharp XRD peak at 143 – 303 K.<sup>6</sup> This suggests a relationship between the size of the confined space and the behavior of water molecular assemblies at low temperature, such as the formation of crystal phases ( $I_c$ ,  $I_h$ , and others) or amorphous solids (LDA; low-density amorphous solids). We could not confirm that a water layer structure formed on the carbon surface at low temperature, since it is difficult to understand the three-dimensional configuration of the hydrogen network in carbon micropores using only XRD methods. We are currently attempting a more detailed analysis of the hydrogen bond network structure in carbon micropores by a combination of XRD and neutron diffraction experiments supported by reverse Monte Carlo simulation.<sup>38-40</sup> Our results, which should clarify the hydrogen bonding structure in carbon micropores, will be discussed in a future article.

#### **4. Conclusion**

Water confined in 1.36 nm carbon micropores exhibited continuously decreasing density with decreasing temperature, or negative thermal expansion, over a wide temperature range below 277 K. XRD and SAXS results revealed that the intermolecular structure of water in the micropores at 298 K was more ordered than that of the bulk state and changed gradually to the  $I_c$ -like structure with decreasing temperature. Thus, we can describe anomalous water structures in carbon micropores at temperatures ranging from ambient to cryogenic by using a combination of XRD and SAXS measurements.

We also proposed a new approach to the density analysis of confined systems in nanospaces using SAXS analysis. The approach enables us to determine the correct density of adsorbed materials in nanospaces and thereby understand the principles of adsorption in nanospaces

more clearly. Moreover, it should be useful for investigating the phase transitions<sup>3</sup> and critical phenomena<sup>10</sup> of condensed material in nanospaces.

This study demonstrates that a combination of XRD and SAXS measurements is a productive method for obtaining micro- and mesoscopic geometric information regarding confined systems in nanospaces.

### Acknowledgements

This research was supported by a Grant-in-Aid for Young Scientists (A) (No. 19685002) from the Ministry of Education, Culture, Sports, Science and Technology, Japan and the Program for Fostering Regional Innovation in Nagano, funded by MEXT, Japan.

### References

1. I. Otsuka and S. Ozeki, *J. Phys. Chem. B*, 2006, **110**, 1509.
2. K. Koga, G. T. Gao, H. Tanaka and X. C. Zeng, *Nature*, 2001, **412**, 802.
3. H. Kyakuno, K. Matsuda, H. Yahiro, Y. Inami, T. Fukuoka, Y. Miyata, K. Yanagi, Y. Maniwa, H. Kataura, T. Saito, M. Yumura and S. Iijima, *J. Chem. Phys.* 2011, **134**, 244501.
4. J. Hernández-Rojas, V. Monteseuro, J. Bréton and J.M. Gomez Llorente, *Chem. Phys.* 2011, in Press.
5. T. Uchida, T. Ebinuma, S. Takeya, J. Nagao and H. Narita, *J. Phys. Chem. B*, 2002, **106**, 820.
6. T. Iiyama, K. Nishikawa, T. Suzuki and K. Kaneko, *Chem. Phys. Lett.*, 1997, **274**, 152.
7. T. Iiyama, Y. Kobayashi, K. Kaneko and S. Ozeki, *Colloids Surf. A*, 2004, **241**, 207.
8. T. Ohba and K. Kaneko, *J. Phys. Chem. C*, 2007, **111**, 6207.

9. S. Agnihortri, P. Kim, Y. Zheng, J. P. B. Mota and L. Yang, *Langmuir*, 2008, **24**, 5746.
10. A. Striolo, K. E. Gubbins, M. S. Gruszkiewicz, D. R. Cole, J. M. Simonson, A. A. Chialvo, P. T. Cummings, T. D. Burchell and K. L. More, *Langmuir*, 2005, **21**, 9457.
11. K. Kaneko, N. Fukuzaki, K. Kakei, T. Suzuki and S. Ozeki, *Langmuir*, 1989, **5**, 960.
12. T. Ohkubo, T. Konishi, Y. Hattori, H. Kanoh, T. Fujikawa and K. Kaneko, *J. Am. Chem. Soc.*, 2002, **124**, 11860.
13. J. Chmiola, G. Yushin, Y. Gogotsi, C. Porter, P. Simon and P. L. Taberna, *Science*, 2006, **313**, 1760.
14. O. Byl, P. Kondratyuk and J. T. Yates Jr., *J. Phys. Chem. B*, 2003, **107**, 4277.
15. C. H. Turner, J. K. Johnson and K. E. Gubbins, *J. Chem. Phys.*, 2001, **114**, 1851.
16. T. Iiyama, K. Nishikawa, T. Suzuki, T. Otowa, M. Hijiriyama, Y. Nojima and K. Kaneko, *J. Phys. Chem. B*, 1997, **101**, 3037.
17. S. J. Gregg and K. S. W. Sing, *Adsorption, Surface Area and Porosity (2nd Ed.)*, Academic Press, London, 1981, p. 248.
18. P. H. Poole, F. Sciortino, U. Essmann, H. E. Stanley, *Nature*, 1992, **360**, 324.
19. O. Mishima, H. E. Stanley, *Nature*, 1998, **392**, 164.
20. F. Mallamace, M. Broccio, C. Corsaro, A. Faraone, D. Majolino, V. Venuti, L. Liu, C. -Y. Mou, S. -H. Chen, *Proc. Natl Acad. Sci. USA*, 2007, **104**, 424.
21. D. Liu, Y. Zhang, Y. Liu, J. Wu, C.-C. Chen, C.-Y. Mou and S.-H. Chen, *J. Phys. Chem. B*, 2008, **112**, 4309.
22. D. Liu, Y. Zhang, C.-C. Chen, C.-Y. Mou, P. H. Poole and S.-H. Chen, *Proc. Natl Acad. Sci. USA*, 2007, **104**, 9570.
23. Y. Zhang, K.-H. Liu, M. Lagi, D. Liu, K. C. Littrell, C.-Y. Mou and S.-H. Chen, *J. Phys. Chem. B*, 2009, **113**, 5007.

24. L. A. Solovyov, V. I. Zaikovskii, A. N. Shmakov, O. V. Belousov and R. Ryoo, *J. Phys. Chem. B*, 2002, **106**, 12198.
25. M. Kaneda, T. Tsubakiyama, A. Carlsson, Y. Sakamoto, T. Ohsuna, O. Terasaki, S. H. Joo and R. Ryoo, *J. Phys. Chem. B*, 2002, **106**, 1256.
26. L. Eliad, G. Stalitra, E. Pollak, A. Sorrer and D. Aurbach, *Langmuir*, 2005, **21**, 10615.
27. K. Kaneko, C. Ishii, M. Ruike and H. Kuwabara, *Carbon*, 1992, **30**, 1075.
28. H. Omichi, T. Ueda, K. Miyakubo and T. Eguchi, *Chem. Lett.*, 2007, **36**, 256.
29. S. Jiang, J. A. Zollweg and K. E. Gubbins, *J. Phys. Chem.*, 1994, **98**, 5709.
30. M. El-Merrai, M. Aoshima and K. Kaneko, *Langmuir*, 2000, **16**, 4300.
31. P. Debye and A. M. Bueche, *J. Appl. Phys.*, 1949, **20**, 518.
32. P. Debye, H. R. Anderson Jr., H. Brumberger, *J. Appl. Phys.*, 1957, **28**, 679.
33. T. Iiyama and S. Ozeki, *Tanso*, 2008, **235**, 275 (in Japanese).
34. *CRC Handbook of Chemistry and Physics*; Taylor and Francis
35. J. E. Bertie, L. D. Calvert and E. Whalley, *J. Chem. Phys.*, 1963, **38**, 840.
36. T. Yamaguchi, H. Hashi and S. Kittaka *J. Mole. Liq.*, 2006, **129**, 57.
37. K. Morishige and H. Uematsu, *J. Chem. Phys.*, 2005, **122**, 44711.
38. A. Tanaka, T. Iiyama, T. Ohba, S. Ozeki, K. Urita, T. Fujimori, H. Kanoh and K. Kaneko, *J. Am. Chem. Soc.*, 2010, **132**, 2112.
39. T. Iiyama, R. Aragaki, T. Urushibara and S. Ozeki, *Adsorpt. Sci. Technol.*, 2006, **24**, 815.
40. T. Iiyama, K. Hagi, T. Urushibara and S. Ozeki, *Colloids Surf. A*, 2009, **347**, 133.

## Figure captions

Fig. 1. The adsorption isotherms of water at 298 K(red) and nitrogen at 77 K(black) on A25.

The closed circles and squares show the adsorption branch and the opened circles and squares show the desorption branch.

Fig. 2. The corrected SAXS profiles of water adsorbed on A25 by  $\phi = 0.85$  at 20 K (red), 120 K (blue), 200 K (black), 225 K (green), 250 K (sky blue), 277 K (purple) and 298 K (light green).

Fig. 3. Debye-Bueche plots of the SAXS profiles of water adsorbed on A25 by  $\phi = 0.85$  at 20 K (red), 120 K (blue), 200 K (black), 225 K (green), 250 K (sky blue), 277 K (purple) and 298 K (light green).

Fig. 4. The temperature dependence of density of confined water on A25 (black), water<sup>31</sup> (red) and ice<sup>31</sup> (blue).

Fig. 5. XRD profiles of water adsorbed on A25 by  $\phi = 0.85$  at 20 K (red), 120 K (blue), 200 K (black), 225 K (green) and 298 K (light green) and A25 under vacuum at 298 K (brawn).

Fig. 6. Corrected XRD profiles of water adsorbed on A25 by  $\phi = 0.85$  at 20 K (red), 120 K (blue), 200 K (black), 225 K (green), 250 K (sky blue), 277 K (purple) and 298 K (light green). XRD profile of  $I_c$  (upward) and  $I_h$  (downward) are also shown.

Fig. 7. Electron radial distribution functions of water adsorbed on A25 by  $\phi = 0.85$  at 20 K (red), 120 K (blue), 200 K (black), 225 K (green), 250 K (sky blue), 277 K (purple) and 298 K (light green) and bulk water at 298 K (black break line).

Table 1 Pore structure of A25 activated carbon fiber

	pore width ( $w / \text{nm}$ )	micropore volume ( $W_0 / \text{ml g}^{-1}$ )	specific surface area ( $a_\alpha / \text{m}^2 \text{g}^{-1}$ )
A25	1.36	1.29	1970

Fig. 1 Iiyama

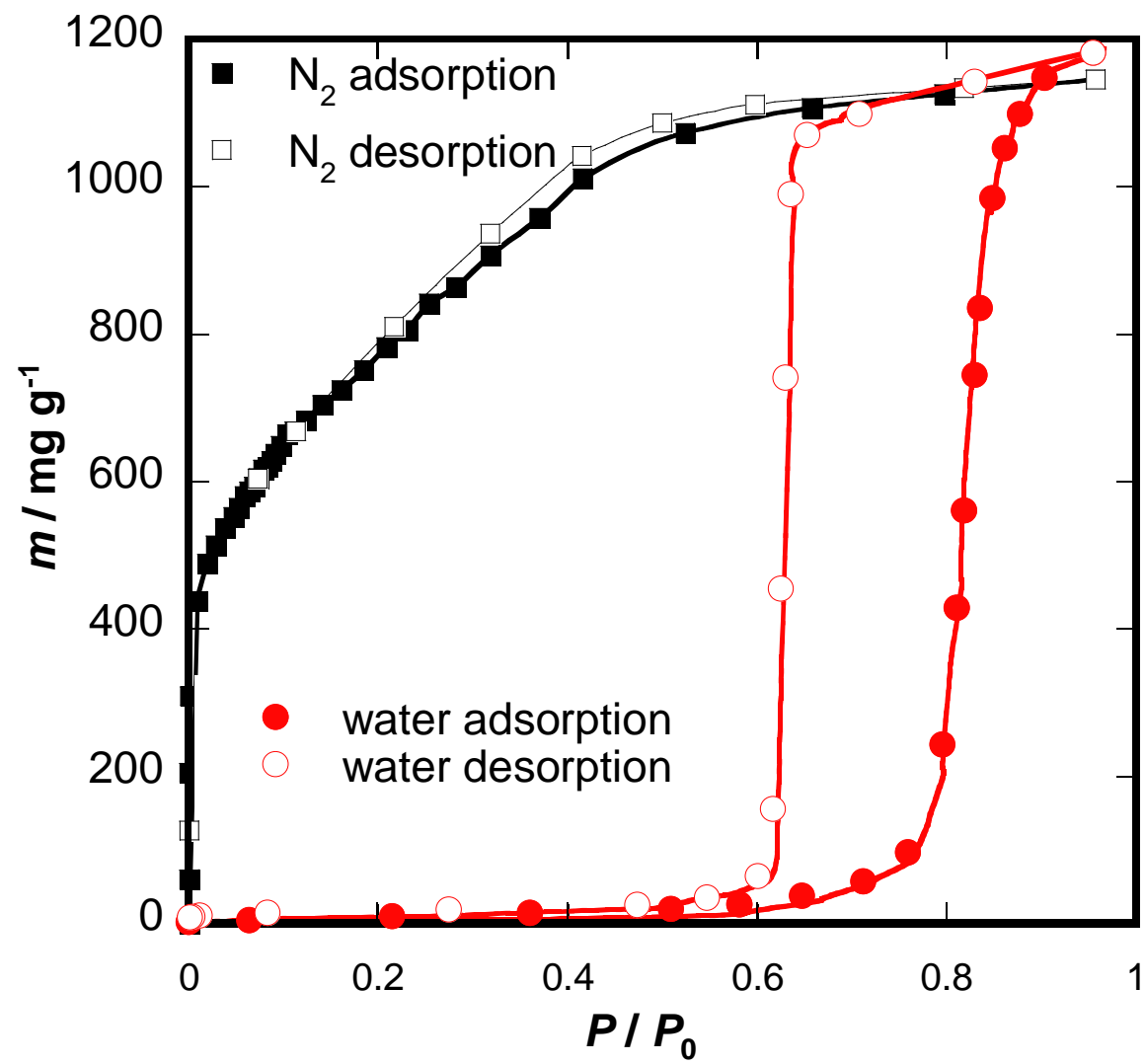


Fig. 2

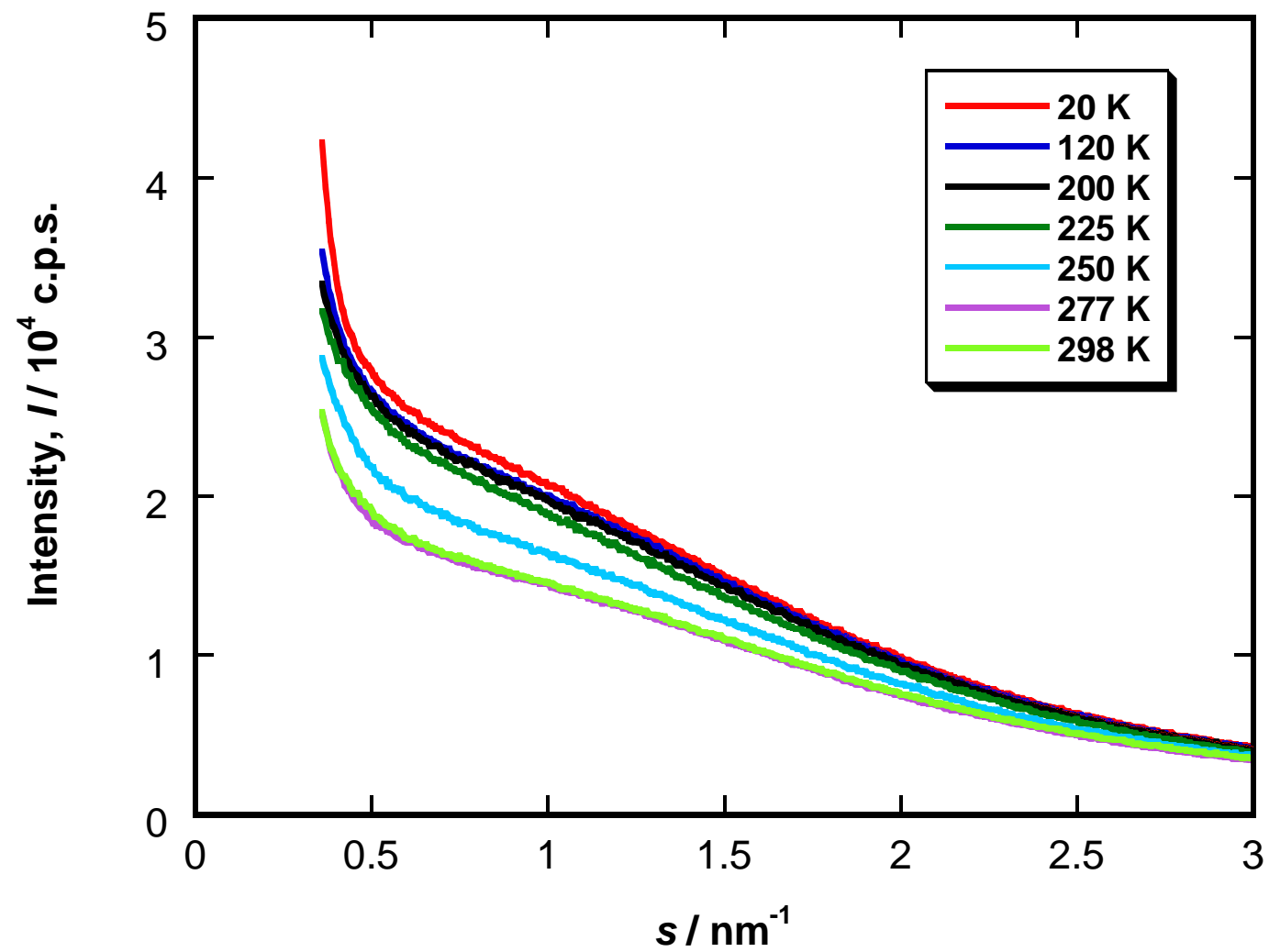


Fig. 3

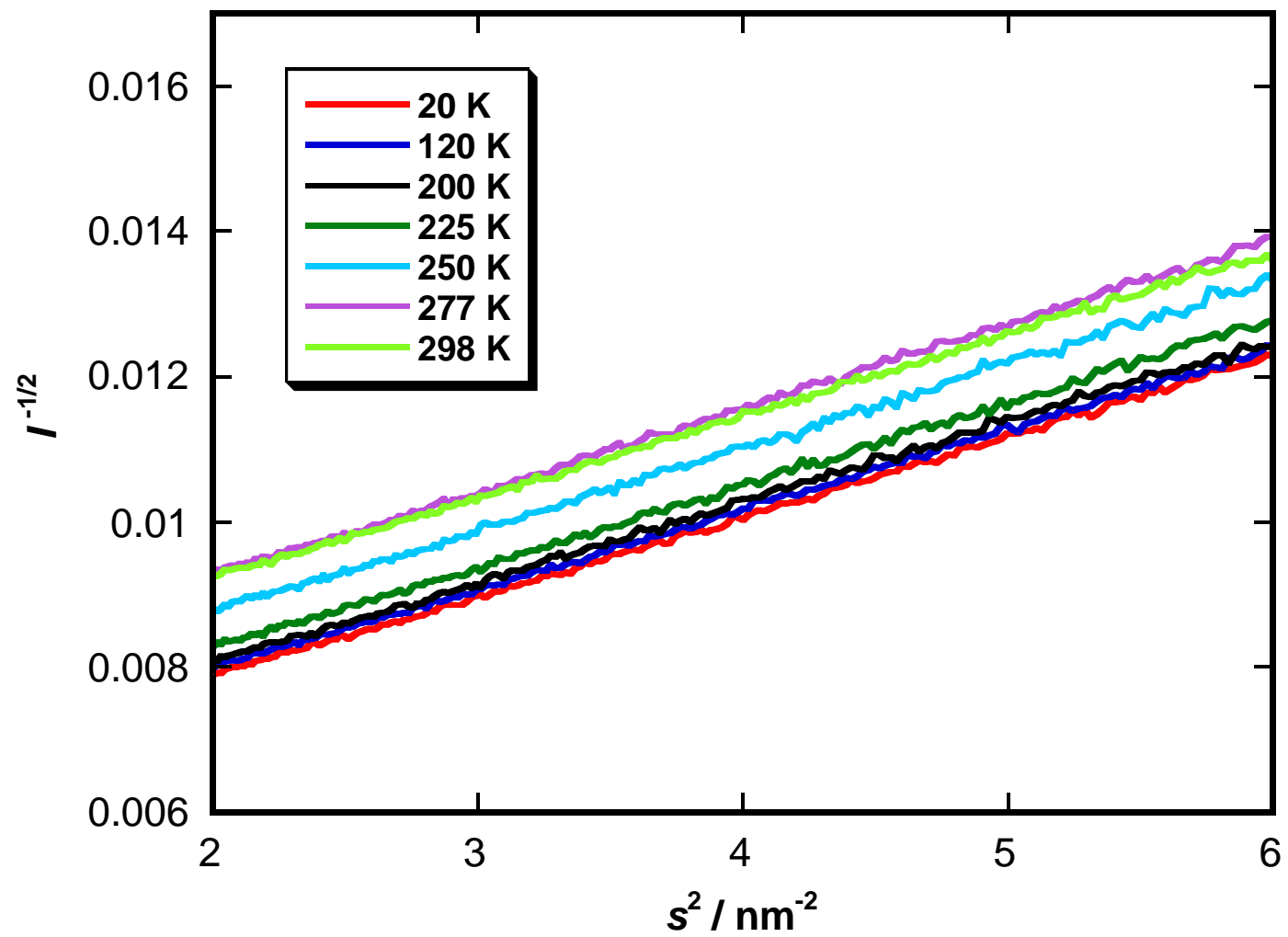


Fig. 4

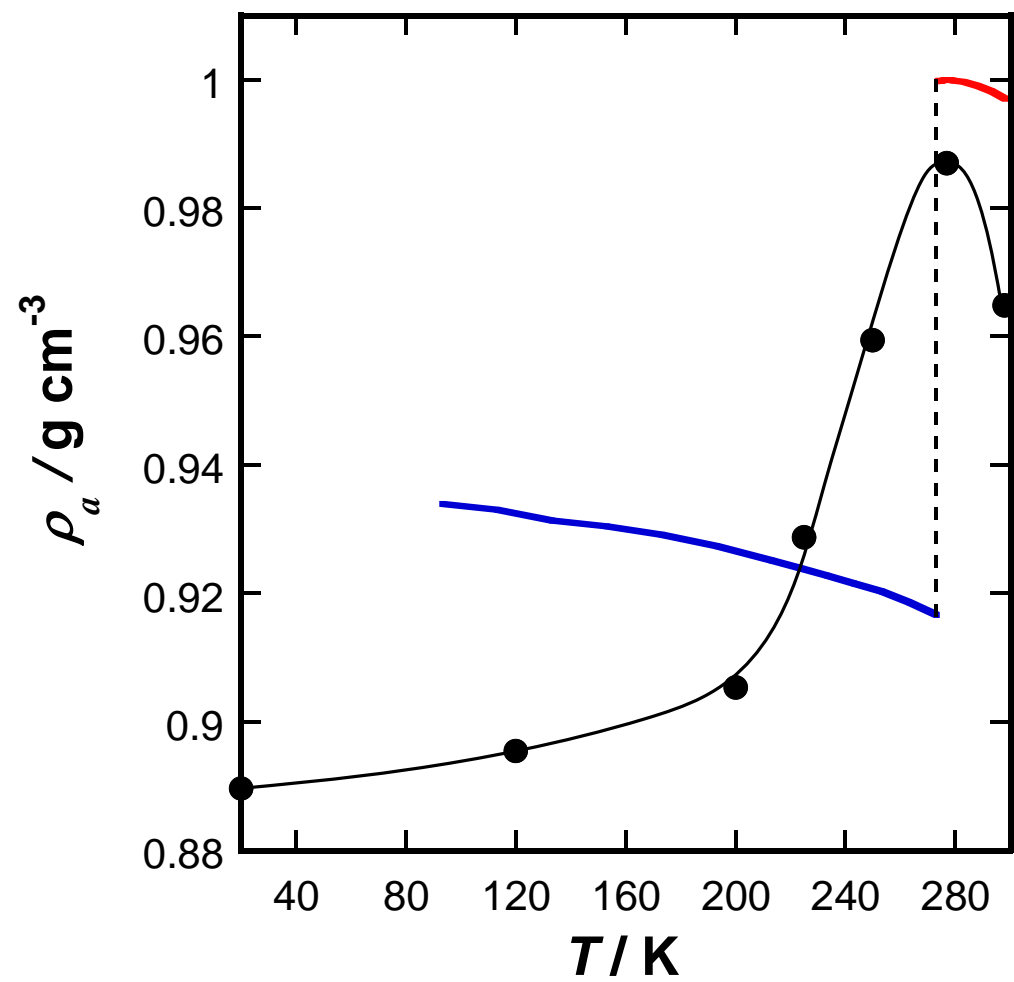


Fig. 5

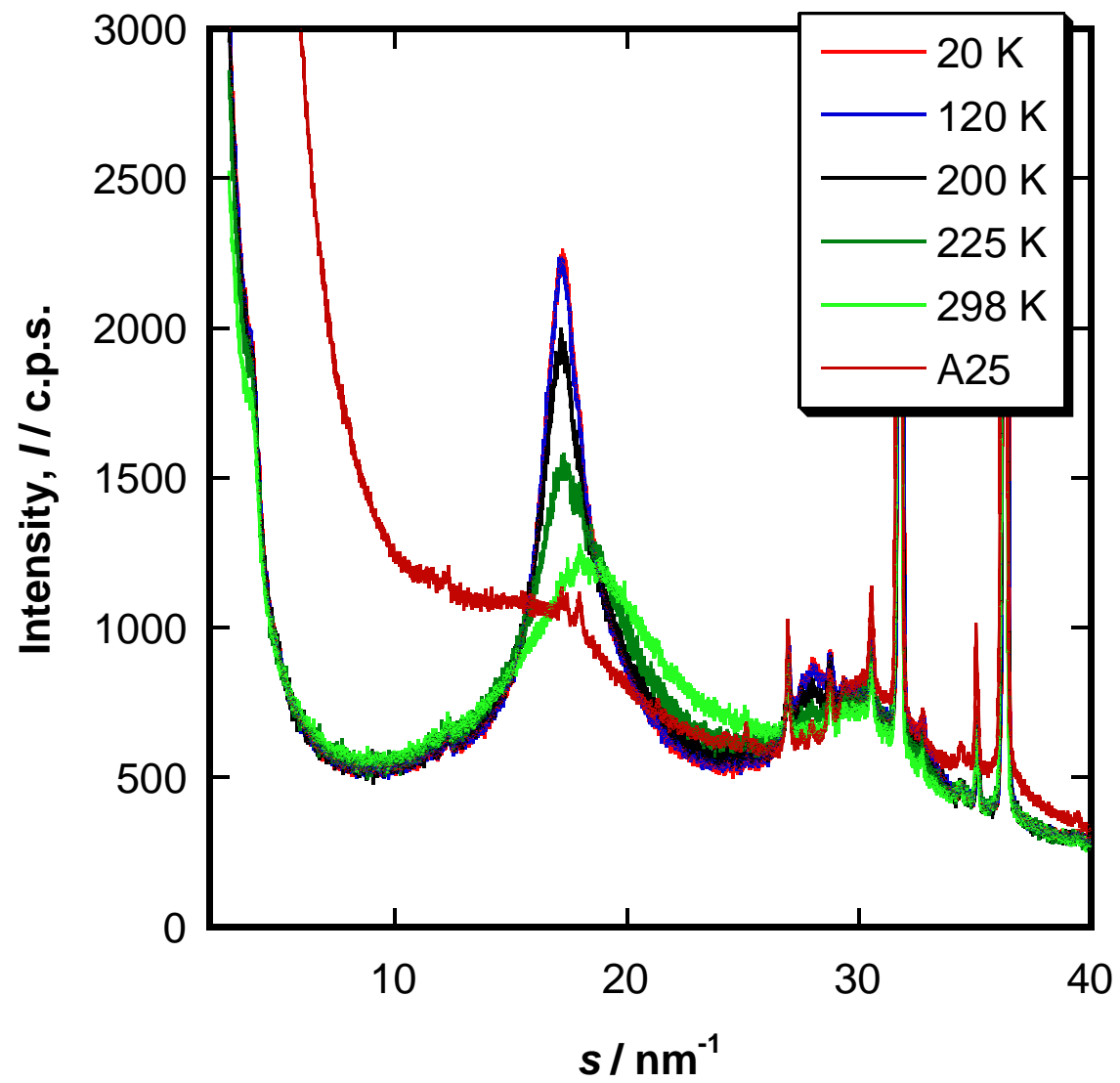


Fig. 6

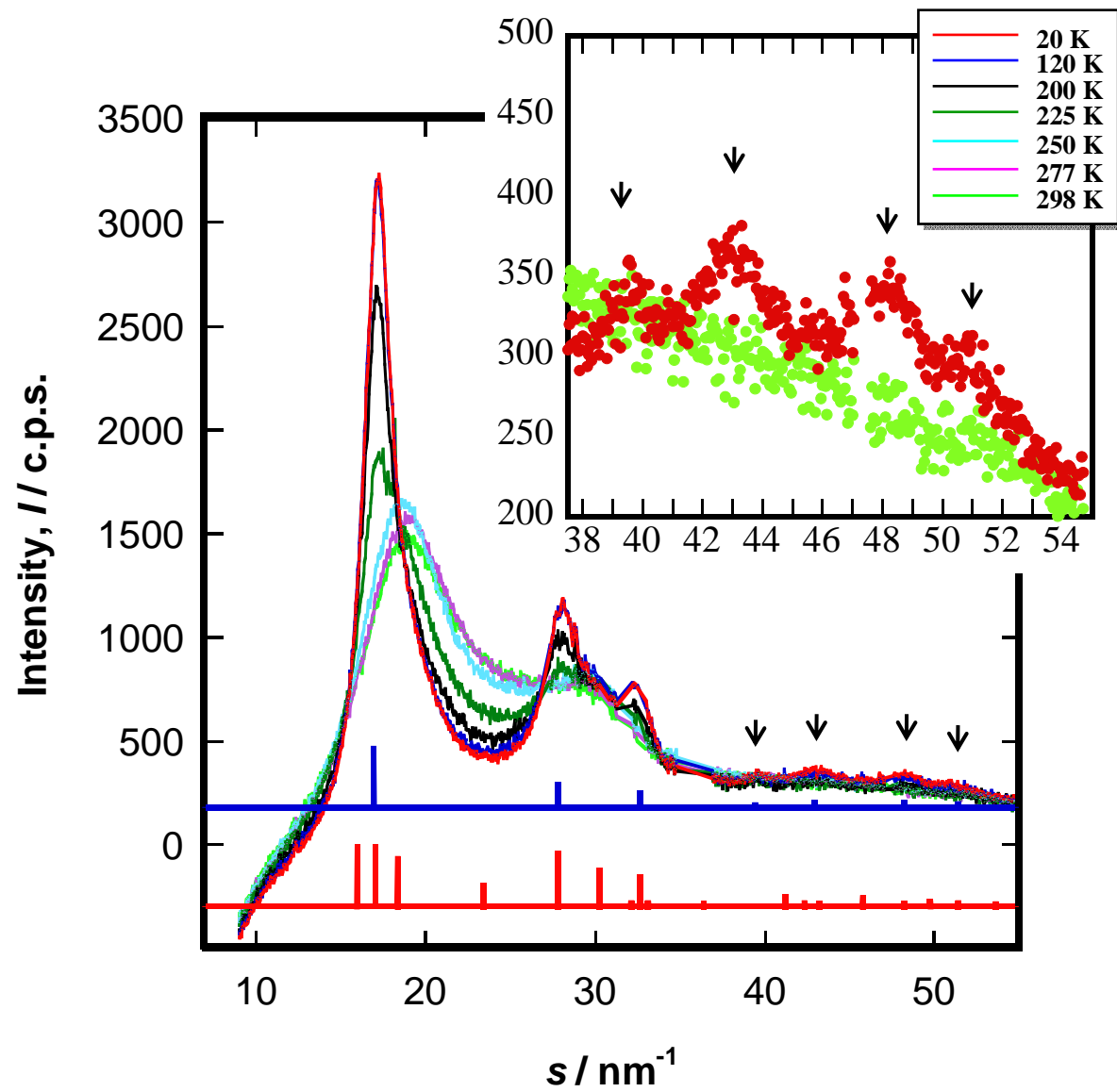
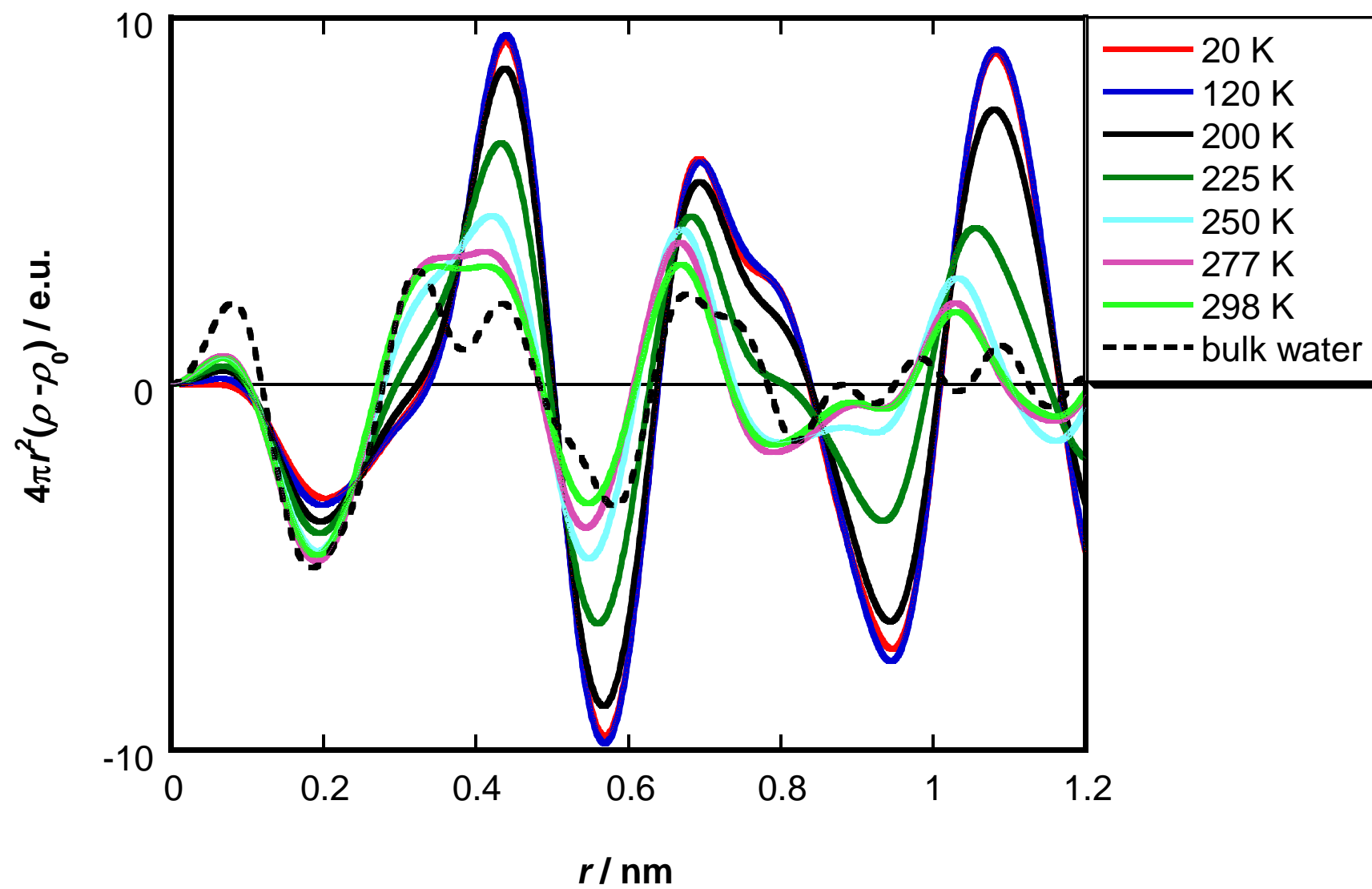


Fig. 7



### Figure captions for supplementary figures

Fig. S1. SAXS profiles of water adsorbed on A25 at 277 K at different amount of adsorbed  $m = 0$  (black), 300 (red), 500(blue), 650(green), 950 (purple) and 1100  $\text{mg g}^{-1}$ (sky blue), respectively.

Fig. S2. Debye-Bueche plots of the SAXS profiles of water adsorbed on A25 by  $\phi = 0.85$  at 20 K (red), 120 K (blue), 200 K(black), 225 K(green), 250 K(sky blue), 277 K(purple) and 298 K (light green).

Fig. S3. The temperature dependence of  $I_0$ , which are determined by Debye-Bueche analysis of SAXS profiles of water adsorbed on A25.

Fig. S4. The temperature dependence of  $\xi$  which are earned by Debye-Bueche analysis of SAXS profiles of water adsorbed on A25.

Fig. S1 (supplement) Iiyama

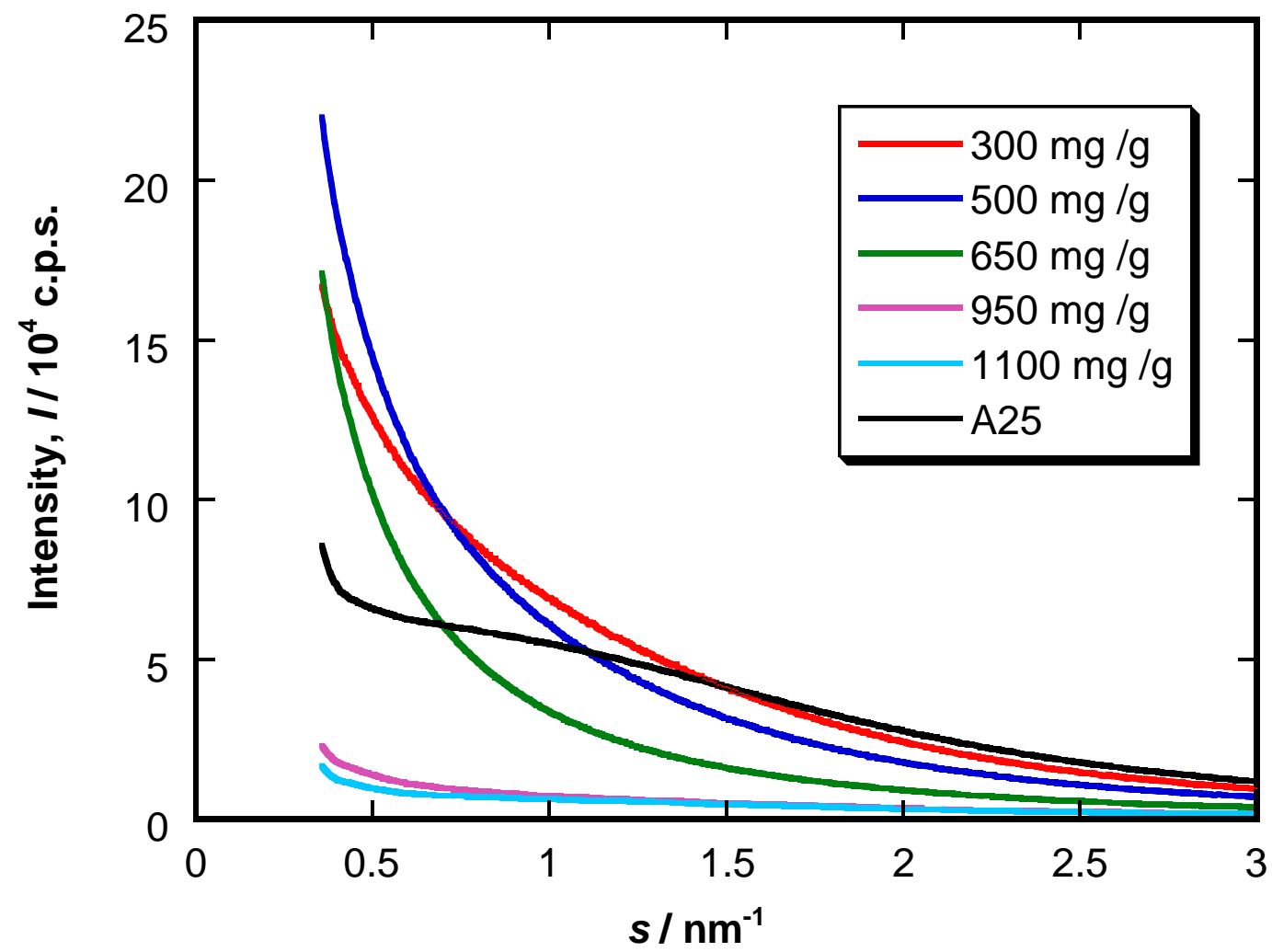


Fig. S2 (supplement)

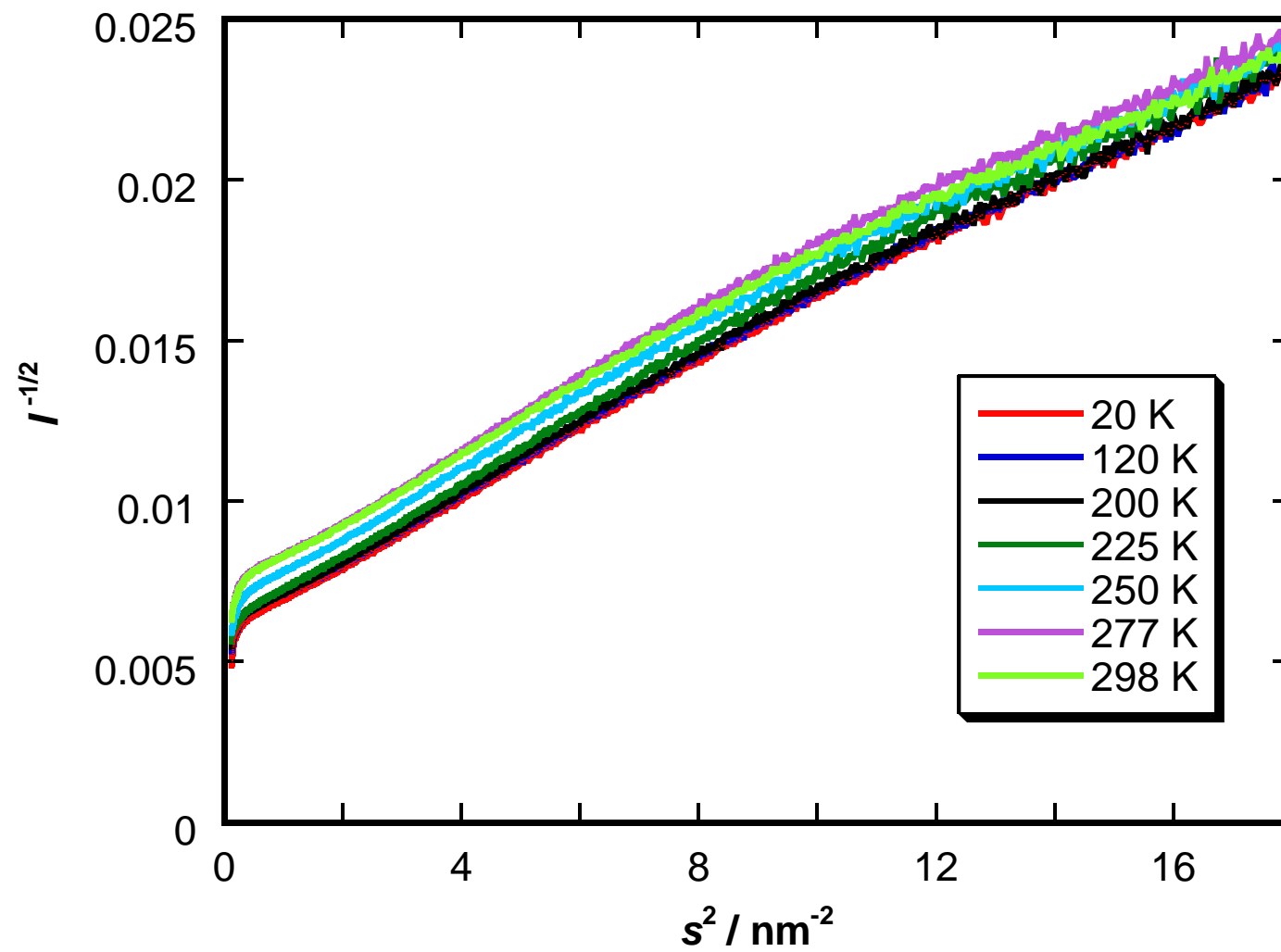


Fig. S3 (supplement)

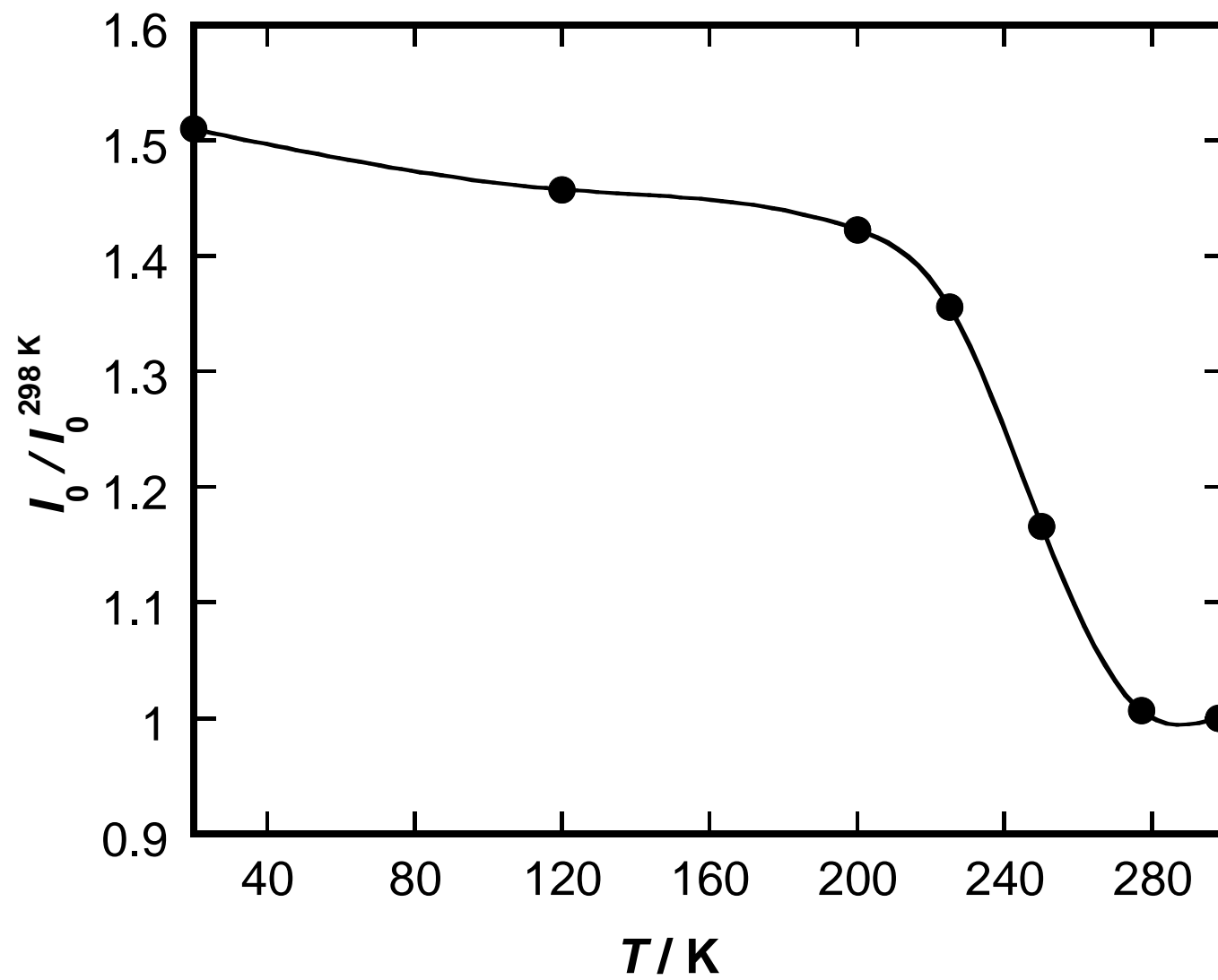
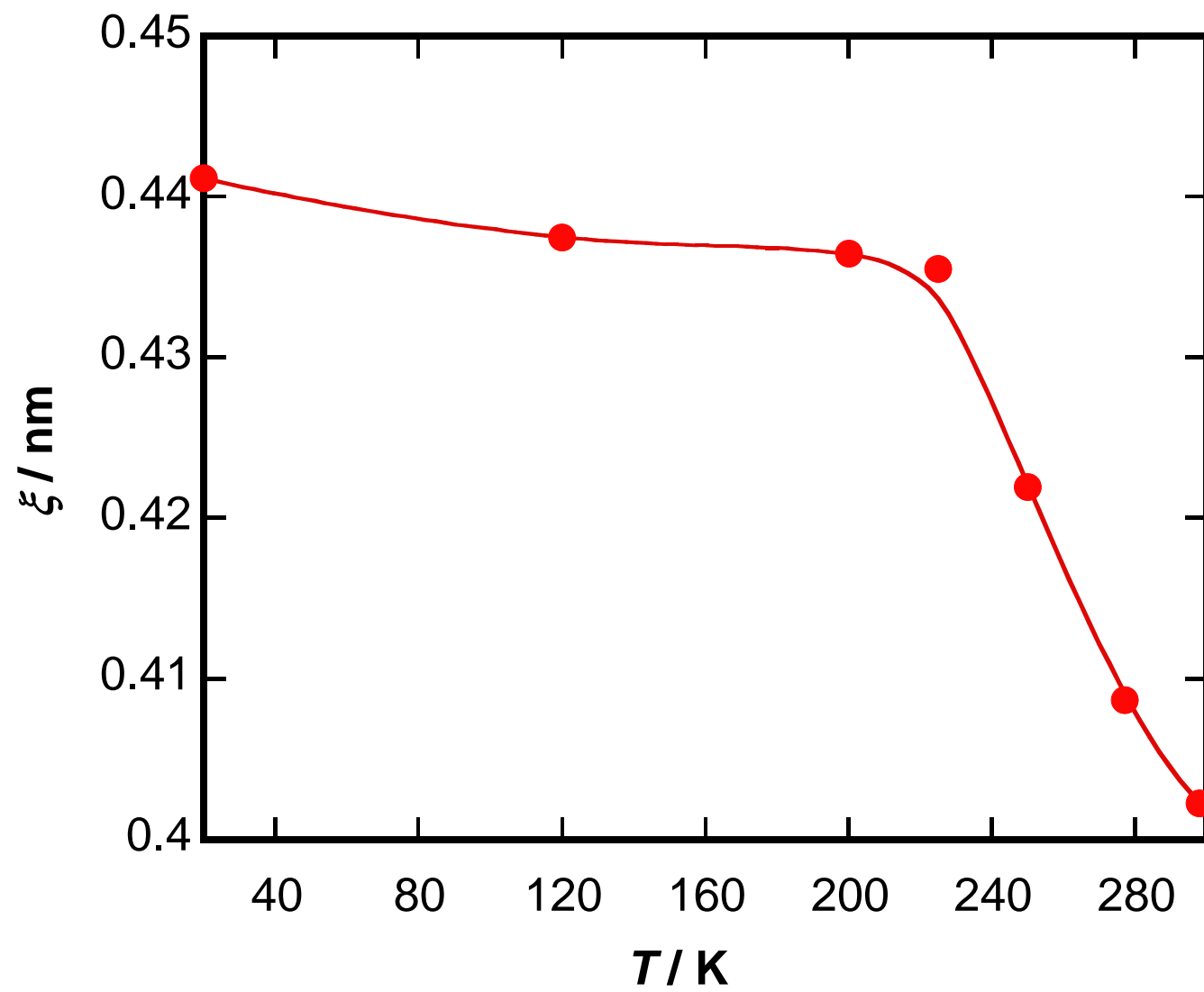
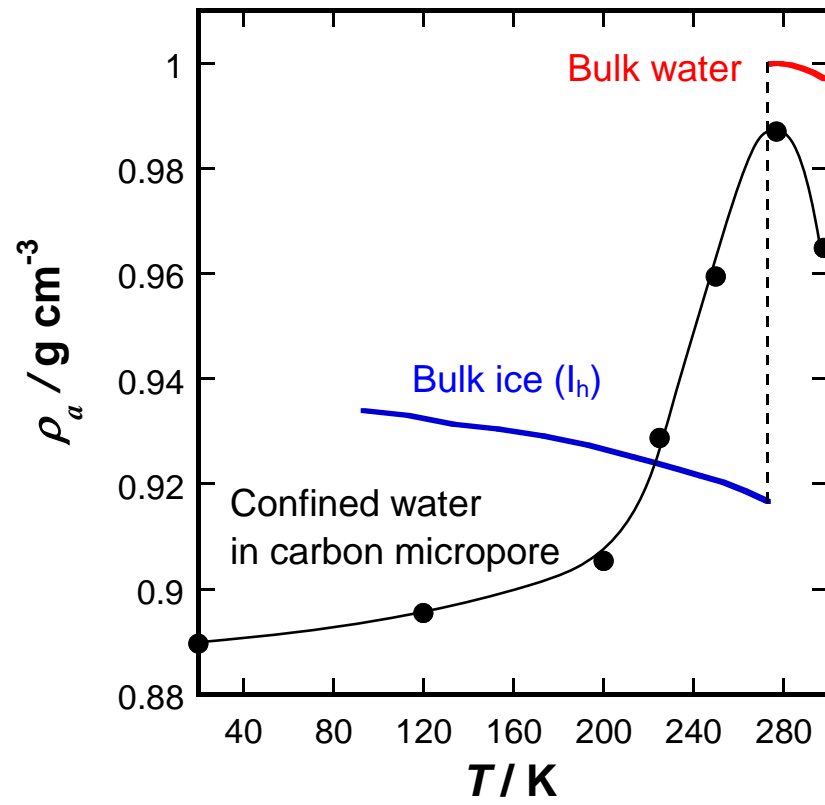


Fig. S4 (supplement)



Graphic Abstract



Density of confined water in carbon micropore of 1.36 nm width